Nematode Sperm Motility: Nonpolar Filament Polymerization Mediated by End-Tracking Motors

Richard B. Dickinson*† and Daniel L. Purich‡
Departments of *Chemical Engineering, †Biomedical Engineering, and ‡Biochemistry & Molecular Biology, Colleges of Engineering and Medicine, University of Florida, Gainesville, Florida

ABSTRACT In nematode sperm cell motility, major sperm protein (MSP) filament assembly results in dynamic membrane protrusions in a manner that closely resembles actin-based motility in other eukaryotic cells. Paradoxically, whereas actin-based motility is driven by addition of ATP-bound actin subunits onto actin filament plus-ends located at the cell membrane, MSP dimers assemble from solution into nonpolar filaments that lack a nucleotide binding site. Thus, filament polarity and on-filament ATP hydrolysis, although essential for actin-based motility, appear to be unnecessary for membrane protrusions by MSP. As a potential resolution to this paradox, we propose a model for MSP filament assembly and force generation by MSP filament end-tracking proteins. In this model, ATP hydrolysis drives affinity-modulated, processive interactions between membrane-associated proteins and elongating filament ends. However, in contrast to the ''actoclampin'' model for actin filament end-tracking motors, ATP activates the tracking protein (or a soluble cofactor) rather than the MSP subunits themselves (in contrast to activation of actin subunits by ATP binding). The MSP end-tracking model predicts properties that are consistent with several key observations of MSP-based motility, including persistent membrane attachment, polymerization of filament ends at the membrane with depolymerization of free-filament ends away from the membrane, as well as a saturating dependence of polymerization rate on the concentration of non-MSP soluble cytoplasmic components.

INTRODUCTION

Cells crawl by polymerizing intracellular filaments to form protrusions at their leading edge, which then adhere to the substratum and allow the cell body to pull itself forward by means of more distal contractile forces (1). The protrusions of most amoeboid cells consist of actin filaments, which bind ATP-actin monomers at their (+)-ends situated at the membrane and release ADP-actin monomers at their (−)-ends away from the membrane. Hydrolysis of filament-bound ATP has been proposed to drive this head-to-tail association/dissociation cycle in a process called ''treadmilling'' (2) and to drive processive monomer addition to elongating filament (+)-ends that are attached to the membrane by filament end-tracking proteins (3,4). Both of these ATP-dependent processes exploit the structural polarity of actin filaments to add ATP-monomers to filament (+)-ends positioned at the membrane surface. Although nematode sperm cell crawling is qualitatively similar (Fig. 1 *a*), these cells do not contain actin filaments (5,6); they instead assemble filaments from a large cytoplasmic pool of major sperm protein (MSP) dimers. Paradoxically, MSP dimers possess a twofold rotational symmetry, form nonpolar filaments, and do not bind ATP (7). Thus, unlike actin assembly, preferential MSP addition to one end of an MSP filament must be driven by external factors (8).

Under intracellular conditions, MSP filaments spontaneously disassemble, suggesting that the solution-phase MSP dimer concentration [M] of ~4 mM (8) is less than the critical concentration $[M]_c$ needed for assembly. From a thermodynamic viewpoint, the free energy ΔG_f for MSP dimer addition to free filament ends is:

$$\Delta G_f = -kT \ln \frac{[M]}{[M]_c}, \quad (1)$$

which must be positive where assembly is energetically unfavorable. Nevertheless, in the presence of ATP, MSP dimers do add to filament ends localized on the membrane surfaces of nematode sperm cells. One explanation offered by Roberts and co-workers (9) is that MSP dimers become activated by membrane-bound components and then diffuse locally to find filament ends before spontaneously deactivating farther from the membrane. Such a mechanism, which conforms to the view that working filaments must have free ends that fluctuate away from a surface to add new subunits (10), forms the basis for protrusive force generation in recent MSP-based motility models (11).

A requirement for both a membrane component and a soluble cofactor in MSP polymerization is suggested by the results of Italiano et al. (12), who examined sperm membrane vesicle propulsion by MSP polymerization in cell extracts (Fig. 1 *b*). In addition to a required membrane component, later identified as a 48-kDa phosphoprotein (13), they diluted the extract to demonstrate that the velocity of propelled vesicles depended on the concentration of soluble cytoplasmic components. However, restoring the concentration of MSP to 4 mM failed to restore the normal speed at any

Submitted June 2, 2006, and accepted for publication September 19, 2006.

Address reprint requests to Dr. Richard B. Dickinson, Dept. of Chemical Engineering, University of Florida College of Engineering, PO Box 116005, Gainesville, FL 32611-6005. Tel.: 352-392-0898; E-mail: dickinso@che.ufl.edu.

0006-3495/07/01/622/10 $2.00

doi: 10.1529/biophysj.106.090472

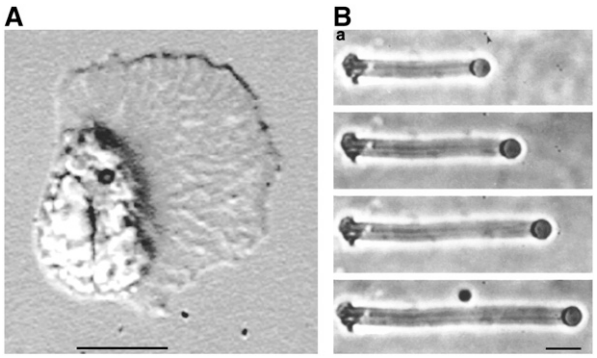

FIGURE 1 Characteristics of nematode sperm cell motility by polymerization of major sperm protein. (*a*) A nematode sperm cell undergoing active cell crawling from left to right (reproduced with permission from Italiano et al. (24)). The fan-like lamellipodial region to the right consists of MSP filaments and fibers polymerizing from the leading membrane edge to extend the lamellipod. Scale bar = 10 μm. (*b*) A sperm cell membrane vesicle is propelled by polymerization of MSP filament ends located at the membrane surface to form a dense MSP filament network. Scale bar = 5 μm. (Reprinted with permission from Italiano et al. (12).)

extract dilution. The latter finding implies that the MSP concentration itself was not rate limiting at any dilution, suggesting instead that the concentration of an unidentified soluble component was rate limiting. Finally, Italiano et al. (12) made the important observation that MSP filaments remain attached to the propelled vesicle during polymerization.

We previously proposed the ''Filament End-Tracking Motor'' mechanism (3,4), a generalizable model in which surface-bound end-tracking proteins advance processively on elongating filaments ends. In this model, nucleotide hydrolysis energy drives affinity-modulated interactions between the end-tracking proteins and filament subunits at or near the terminus. The end-tracker mechanism permits rapid elongation of tethered filaments under conditions where elongation of free ends would be thermodynamically unfavorable, such as when the monomer concentration is near or below its critical concentration and/or when pushing against a significant load (several piconewtons). The model also explains a likely role of soluble cofactors such as profilin in the affinity modulation step, consistent with processive elongation of actin filaments by formins in the presence of profilin-actin-ATP (14).

TABLE 1 Definitions and values of model parameters

Symbol	Definition
d	Added filament length per subunit (3 nm)
F	Force (pN)
K_h	ATP conversion equilibrium constant
$K_{X\cdot Y}$	Equilibrium dissociation constant for protein X binding to protein Y
$K_{XY\cdot Z}$ or $K_{Z\cdot XY}$	Equilibrium dissociation constant for protein complex X·Y binding to protein Z
$K_{X\cdot Y\cdot Z}$	Equilibrium dissociation constant of forming the protein complex X·Y·Z from proteins X, Y, and Z ($= K_{X\cdot Y}K_{XY\cdot Z} = K_{Y\cdot Z}K_{X\cdot YZ} = K_{X\cdot Z}K_{XZ\cdot Y}$)
$k_{X\cdot Y}$	Association rate constant for X binding to Y (s^{-1} or $\mu M^{-1}s^{-1}$)
$k^-_{X\cdot Y}$	Rate constant for X dissociation from Y (s^{-1} or $\mu M^{-1}s^{-1}$)
kT	Boltzmann constant × temperature (4.1 pN-nm)
M	MSP dimer
r	Polymerization rate (s^{-1})
r_c	Rate of formation of T·M or T·M·S complex (s^{-1})
r_t	Rate of direct transfer to filament end (s^{-1})
S	Soluble cofactor
T	Tracking unit

Clearly, end-tracking motors driven by on-filament ATP hydrolysis cannot explain nematode sperm motility, because MSP filaments are nonpolar and lack an ATPase activity. Nevertheless, polymerization and motility by MSP filaments and actin filaments share several properties that are anticipated by the end-tracking mechanism (8): a), subunit addition to filament ends is thermodynamically favored at the membrane, whereas disassembly is favored in the bulk cytoplasm away from the membrane; b), ATP is required for filament assembly at the membrane surface; c), MSP filament ends remain persistently attached to the membranes of propelled vesicles during both protrusion and retraction phases (12,15); d), membrane-bound (13) and soluble protein components (16) are required in addition to MSP and ATP for motility; e), the elongation rate shows rate saturation with respect to MSP concentration (12); and f), both MSP and actin form double-stranded helical filaments (7). These shared properties of actin-based and MSP-based motility are unlikely to be coincidental. We show here that subunit addition and resultant force generation by MSP can be explained by a filament end-tracking mechanism that is functionally analogous to that previously proposed for actin-based motility (3,4). The only mechanistic difference is that the ATPase activity resides with the membrane-bound end-tracking units or with a soluble cofactor. Here, ATP hydrolysis energy activates these other components to modulate end-tracking binding interactions and to facilitate processive dimer addition under conditions where addition to free-filament ends would be thermodynamically unfavorable. This self-consistent mechanism extends the filament end-tracking motor concept to MSP polymerization during nematode sperm cell motility.

Thermodynamics of end-tracking polymerization of nonpolar filaments

The essential elements of an MSP filament end-tracking motor (Fig. 2) include membrane-bound tracking units interacting with the two MSP subfilaments, either without (Mechanism-1 in Fig. 2 *a*) or with (Mechanism-2 in Fig. 2 *b*) participation of a soluble cofactor. Like in the end-tracking cycles proposed in Dickinson et al. (4), the energy of ATP hydrolysis is captured by activating a protein species involved in the cycle to a higher energy state (indicated by * in the notation below), and the release of this energy upon

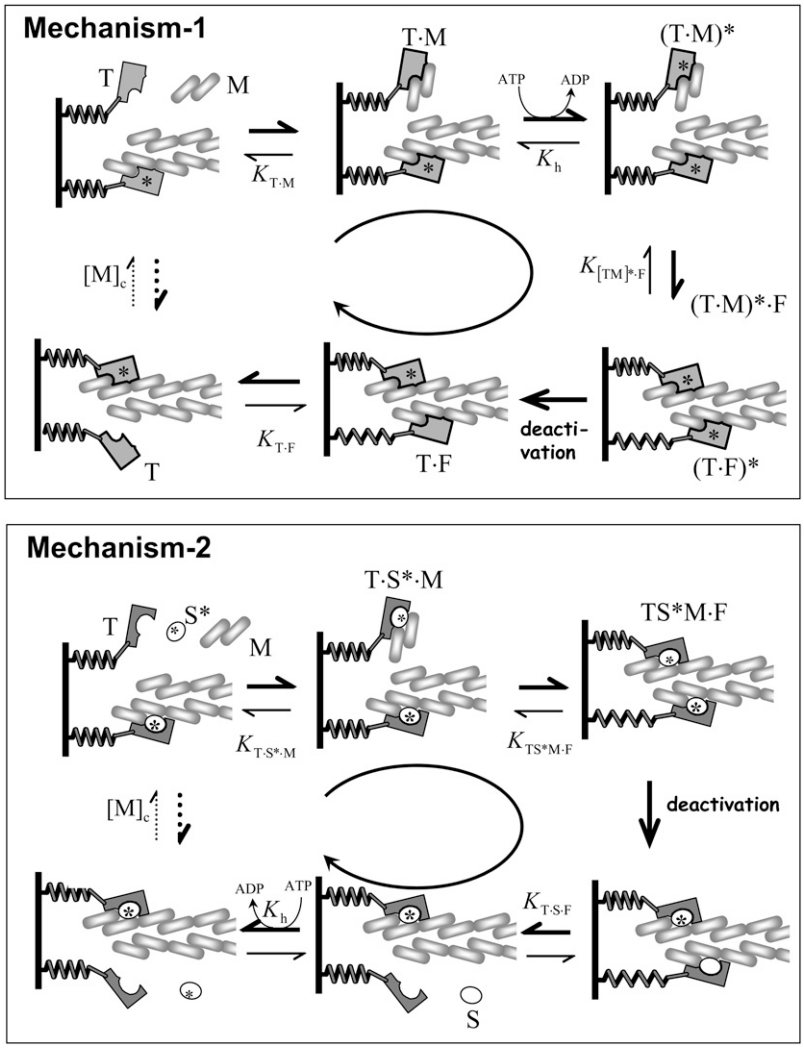

FIGURE 2 Two possible mechanoenzymatic cycles for MSP polymerization from a surface by filament end-tracking motors. Mechanism-1 (proceeding *from upper left* around *to lower left*): the activated tracking unit (*T*) binds an MSP dimer (*M*) from solution. The T·M complex is then activated by ATP (either by nucleotide exchange with ADP or by covalent modification) to form an activated complex (T·M)*, which then binds to the filament end (*F*) to transfer the dimer to the filament (i.e., to form (T·M)*·F). This event triggers the transition of the activated complex on the adjacent subfilament to a lower energy state (i.e., (T·M)*F to T·F), with the released energy going to attenuate the affinity of T for the adjacent subfilament, resulting in its release. Mechanism-2 (proceeding *from upper left* around *to lower left*): an activated soluble cofactor S* and an MSP dimer bind to the tracking unit to form the T·S*·M complex, which then binds to the subfilament end to transfer the dimer (i.e, to form T·S*·M·F). This event triggers deactivation of S* to S, thereby releasing its energy, which goes to disrupt the adjacent tracking unit complex (T·S·F) by attenuating the affinity of one or more of the protein-protein interactions between T, S, and F.

deactivation goes to modulate the affinity of binding interactions and facilitate the net cycle of subunit addition. Mechanism-1 resembles the ''direct-transfer end-tracking motor'' described by Dickinson et al. (4), except that the end-tracking unit, rather than the filament subunits, are activated by ATP. Mechanism-2 resembles the ''cofactor-assisted, direct-transfer end-tracking motor'' described in Dickinson et al. (4), except that the soluble cofactor is activated by ATP.

In Mechanism-1, an MSP dimer (M) binds to the tracking unit (T). (Definitions of symbols and parameters are summarized in Table 1.) The resulting T·M complex is then converted to a higher-energy state (T·M)* by a reaction that utilizes the energy of ATP hydrolysis, thereby converting ATP to ADP. This activation step may be achieved, for example, by exchange of ATP for ADP bound to the T·M complex, or by covalent modification (e.g., phosphorylation or adenylylation) of T. Deactivation later in the cycle would then be achieved by hydrolysis of the bound ATP (or by dephosphorylation or deadenylylation of T). Following activation, the (T·M)* complex binds the dimer to the subfilament end (F), an event that triggers release of the other tracking unit from the adjacent subfilament. In this manner, the energy released upon (T·M)* deactivation is used to attenuate T's affinity for the filament. This energy can be released by either a), deactivation on the same subfilament upon binding of a new subunit onto the other subfilament; or b), deactivation of the newly bound subunit on the other subfilament. Notably, these two possibilities are thermodynamically and functionally equivalent, thus we do not discriminate between the two pathways in this analysis. (Only the latter pathway is illustrated in Fig. 2).

Mechanism-2 is similar, except that the energy driving the cycle is carried by a soluble cofactor S, which is activated by ATP in solution to form the higher-energy species S*. In this cycle, M and S* both bind to T (either in sequence or as a complex), to form T·S*·M, which then binds to F to incorporate the dimer into the subfilament. This event triggers deactivation of S* (on the same or opposite subfilament), causing release of the tracking unit and recycling of S back to solution, where it can be reactivated to S* by ATP (e.g., by nucleotide exchange or covalent modification). Although thermodynamically and functionally similar to Mechanism-1,

Mechanism-2 offers a potential kinetic advantage, in that reactivation of S to S* by ATP can occur rapidly in a solution-phase reaction that is uncoupled from the elongation itself. In contrast, the cycle in Mechanism-1 must await the activation step of (T·M) to (T·M)*. Moreover, Mechanism-2 requires only the release of T to proceed, and the dissociation rate of S from the filament sides may be slower than the elongation rate without impeding the cycle.

An important property shared by both schemes in Fig. 2 is that filament assembly is processive; i.e., at last one strong binding interaction between T and the filament is maintained at each step throughout the cycle, thereby maintaining the purchase of the elongating filament end by the membrane surface. Another important property is that the capture of ATP hydrolysis energy in the net dimer-addition cycle provides a net thermodynamic driving force only for polymerization on the end-tracked filament end, while maintaining a simultaneous net driving force for depolymerization on the opposite free-filament end located away from the membrane.

Molecular stiffness, represented by the springs in Fig. 2, may affect the kinetic rate constants as well as the equilibrium constants of the individual steps, and it can also influence the sensitivities of the cycle to force, as analyzed below.

To illustrate the predicted thermodynamic properties of end-tracked elongation of nonpolar filaments, we first examine the energetics of Mechanism-1. The various equilibrium dissociation constants are defined in Fig. 2 *a*. (The notation $K_{X\cdot Y}$ represents the equilibrium dissociation constant for X binding to Y). The net free energy required for the dimer-addition cycle is

$$\Delta G = -kT\ln\frac{[M]}{K_{T\cdot M}} - kT\ln\frac{[ATP]}{[ADP]K_h} - kT\ln\frac{1}{K_{(TM)^*\cdot F}} - kT\ln K_{T\cdot F}, \quad (2)$$

where K_h is the equilibrium constant for the (T·M)-to-(T·M)* activation reaction (i.e., the required ATP/ADP ratio for states (T·M) to (T·M)* to be equally probable). (Note that, if phosphate is liberated in the activation reaction, K_h will be a proportional to the intracellular phosphate concentration, but not so for simple ATP/ADP exchange). By combining terms, Eq. 2 can be rewritten as

$$\Delta G = -kT\ln\frac{[M]K_{T\cdot F}}{K_{T\cdot M}K_{(TM)^*\cdot F}} - kT\ln\frac{[ATP]}{[ADP]K_h}. \quad (3)$$

We can relate ΔG to the critical concentration $[M]_c$, noting that without the energy yielded by inactivation, detailed balance would require that the energy change of the net cycle be equal to ΔG_f. In this hypothetical case

$$\Delta G_f = -kT\ln\frac{[M]}{[M]_c} = -kT\ln\frac{[M]K_{(T\cdot F)^*}}{K_{(T\cdot M)^*}K_{(TM)^*\cdot F}}, \quad (4)$$

where the constants appearing in Eq. 4 are the corresponding equilibrium dissociation constants for the activated states, with $K_{(T\cdot F)^*}$ corresponding to $K_{T\cdot F}$, $K_{(T\cdot M)^*}$ corresponding to $K_{T\cdot M}$, and $K_{(TM)^*\cdot F}$ corresponding to $K_{TM\cdot F}$. Equation 4 implies $[M]_c K_{(T\cdot F)^*} = K_{(T\cdot M)^*}K_{(TM)^*\cdot F}$, and combining Eq. 2 with Eq. 4 yields

$$\Delta G = -kT\ln\frac{[M]}{[M]_c} - kT\ln f - kT\ln\frac{[ATP]}{[ADP]K_h} - kT\ln\frac{K_{(T\cdot M)^*}}{K_{(T\cdot M)}}, \quad (5)$$

where the factor $f \equiv K_{T\cdot F}/K_{(T\cdot F)^*}$ represents the degree of affinity modulation of T binding to F caused by conversion of (T·M)* to (T·M). The magnitude of f, which reflects the thermodynamic driving force for polymerization, is constrained by the energy released by intracellular ATP hydrolysis, $\Delta G_{ATP\rightarrow ADP}$ ($\sim$22 kT, assuming typical intracellular conditions [ATP]/[ADP] $\sim$ 20, and $[P_i] \sim 1$ mM). The upper bound on f can be found at the limit where all of the energy released upon inactivation goes to modulate $K_{T\cdot F}$. The net effect of the cycle is to hydrolyze one ATP and to add one subunit. Therefore, upon applying Eqs. 1 and 5, the inequality $-\Delta G \leq -\{\Delta G_{ATP\rightarrow ADP} + \Delta G_f\}$ implies

$$f \leq \frac{[ATP]}{[ADP]K_h}\frac{K_{(T\cdot M)^*}}{K_{(T\cdot M)}}e^{-\Delta G_{ATP\rightarrow ADP}/kT}. \quad (6)$$

As indicated in Eq. 5, ATP could fuel one or more important steps in the cycle: i), affinity modulation to release T; ii), activation of T·M to (T·M)*; and iii), storage of energy in the filament to maintain $[M]_c \gg [M]$. The multiple roles for ATP hydrolysis energy are analogous to those in the actoclampin filament end-tracking cycle (4), in which a fraction of ATP hydrolysis energy ($\sim$8 kT) goes to release and recycle ADP-bound subunits from (−)-ends and another goes to facilitate profilin-assisted nucleotide exchange, leaving the remaining energy ($\sim$14 kT) for affinity modulation.

Similar thermodynamic conclusions can be obtained for Mechanism-2 in Fig. 2 *b*, in which an activated soluble cofactor S* undergoes a transition to its deactivated form S following dimer transfer to the filament, resulting in a lower affinity of the tracking unit for the filament end. As in Mechanism-1, the trigger for deactivation may vary without functionally affecting the cycle; i.e., S* could be deactivated immediately upon binding to the filament with the energy released going to detach the tracking unit on the other subfilament, or deactivation of S* could instead await binding of the next subunit (which is the case shown in Fig. 2). The free energy released by one cycle of MSP dimer addition by the cofactor-assisted end-tracking motor is given by:

$$\begin{aligned}\Delta G &= -kT\ln\frac{[M][S^*]}{K_{T\cdot S^*\cdot M}} - kT\ln\frac{1}{K_{TS^*M\cdot F}} - kT\ln\frac{K_{T\cdot S\cdot F}}{[S]} - kT\ln\frac{[ATP][S]}{[ADP][S^*]K_h} \\ &= -kT\ln\frac{[M]K_{T\cdot S\cdot F}}{K_{T\cdot S^*\cdot M}K_{TS^*M\cdot F}} - kT\ln\frac{[ATP]}{[ADP]K_h}, \end{aligned} \quad (7)$$

where $K_{T\cdot S^*\cdot M}$ is the equilibrium dissociation constant of forming the complex T·S*·M from individual species T, S*,

and M, and $K_{T\cdot S\cdot F}$ is likewise defined for binding of T, S, and F to form the complex T·S·F. In this cycle, ATP hydrolysis potentially fuels the end-tracking cycle both by modulating affinity and by increasing the solution-phase concentration of S* relative to S. If hydrolysis were not coupled to MSP dimer addition, detailed balance would require

$$\Delta G_f = -kT \ln \frac{[M]}{[M]_c} = -kT \ln \frac{[M]K_{T\cdot S^*\cdot F}}{K_{T\cdot S^*\cdot M}K_{TS^*M\cdot F}}. \quad (8)$$

Hence, $[M]_c K_{T\cdot S^*\cdot F} = K_{TS^*M\cdot F}K_{T\cdot S^*\cdot M}$. Combining this relation with Eq. 7 yields an expression similar to Eq. 4:

$$\Delta G = -kT \ln \frac{[M]}{[M]_c} - kT \ln f - kT \ln \frac{[ATP]}{[ADP]K_h}, \quad (9)$$

where now the affinity-modulation factor $f \equiv K_{T\cdot S\cdot F}/K_{T\cdot S^*\cdot F}$ is again limited by the total ATP hydrolysis energy. In this case, $-\Delta G \leq -\{\Delta G_{ATP\rightarrow ADP} + \Delta G_f\}$ implies $f \leq ([ADP]K_h/[ATP])e^{-\Delta G_{ATP\rightarrow ADP}/kT}$.

Detailed balance also holds with respect to the different pathways that form the ternary complex T·S*·F:

$$K_{T\cdot S^*\cdot F} = K_{S^*\cdot F}K_{T\cdot S^*F} = K_{T\cdot F}K_{TF\cdot S^*} = K_{T\cdot S^*}K_{TS^*\cdot F}. \quad (10)$$

That is, the net free-energy change upon formation of the ternary complex T·S*·F from T, S* and F, is independent of the pathway, whether a), formation of S*·F, followed by binding of T to S*·F; b), formation of T·F, followed by binding of S*; or c), formation of T·S* followed by binding of T·S* to F. Equation 10 suggests two different ways by which affinity modulation can increase $K_{T\cdot S^*\cdot F}$ to $K_{T\cdot S\cdot F}$ to facilitate the net cycle: by releasing the tracking unit (either as T or T·S) from filament (i.e., increasing $K_{TS\cdot F}$ or $K_{T\cdot SF}$), or by reducing the affinity of S for T to clear S from T, thereby allowing binding of new activated S* (i.e., increasing $K_{T\cdot S^*}$). With respect to the former case, it should be noted that S need not necessarily depart immediately from the filament for the next cycle to proceed. This and other potential kinetic advantages of cofactor-assisted mechanism are discussed in more detail in the following section.

Kinetics of end-tracking polymerization of nonpolar filaments

Although a quantitative prediction of the polymerization rate of end-tracked MSP filaments is not possible without parameter values, the above end-tracking cycles do anticipate certain relevant kinetic limits that can be compared to observations. Based on the results of Italiano et al. (12), we assume that MSP dimers are present in saturating quantities such that the concentration [M] is not rate limiting. We also assume that the dissociation of T and the reactivation of (T·M)* or S* are events that are strongly energetically favored ($[ADP]K_h/[ATP] \gg 1$ and $K_{T\cdot F} \gg 1$) and occur rapidly relative to the rate of dimer loading onto the filament. As shown in the Appendix, these assumptions lead to a Michaelis-Menten-like rate expression

$$r \approx \frac{r_c}{1 + \frac{r_c}{r_t}}, \quad (11)$$

where r_c is the rate of formation of (T·M)* in Mechanism-1 or T·S*·M in Mechanism-2, and r_t is the transfer rate of the dimer to the filament end (i.e., $r_t = k_{TM\cdot F}$ for Mechanism-1 and $r_t = k_{TSM\cdot F}$ for Mechanism-2).

In Mechanism-1, at high concentration of M, the formation of T·M should occur quickly, such that r_c should be governed by the rate of (T·M) activation to (T·M)*. We assume this reaction requires a solution-phase enzyme E, which would be the necessary soluble component implied by the results of Italiano et al. (12). In this case, $r_c = k_a[E]$, with rate constant k_a such that a polymerization rate r in Eq. 11 is a saturating function of [E], characteristic of Michaelis-Menten enzyme kinetics.

In contrast, r_c for Mechanism-2 in the limit of large [M] is predicted to be a saturating function of the total cofactor concentration, $[S]_0$, for the two pathways of T·S*·M formation considered in the Appendix. For the case where S* binds M in solution to saturation (i.e., $[M] \gg K_{S^*\cdot M}$), but M cannot bind T in the absence of S ($K_{T\cdot M}^{-1} = 0$), r_c is given by

$$r_c = k_{T\cdot SM}[S^* \cdot M] \cong k_{T\cdot S^*M}[S]_0. \quad (12)$$

Here, $k_{T\cdot S^*M}$ is the forward binding rate constant for binding of S*·M to T, and $[S]_0$is the total concentration of S. Similarly, for the case where S* and S cannot bind M in solution (i.e., $K_{S^*\cdot M}^{-1} = 0$), but the T·S*·M complex is instead formed by S*-binding to the existing T·M complex ($[M] \gg K_{T\cdot M}$),

$$r_c = k_{TM\cdot S}[S]_0, \quad (13)$$

where $k_{TM\cdot S}$ is the forward rate constant for this binding reaction. Importantly, when the transfer step is fast relative to T·S*·M formation (i.e., $r_t \gg r_c$), both mechanisms predict r to be a saturating function of the cytoplasm extract protein concentration ([E] for Mechanism-1, but $[S]_0$ for Mechanism-2), consistent with the experimental data of Italiano et al. (12) (Fig. 3).

To confirm that this explanation is quantitatively reasonable in terms of Mechanism-2, Eq. 11 is recast as

$$\frac{r}{r_t} \approx \frac{k_+[S]_0}{r_t + k_+[S]_0}, \quad (14)$$

where $k_+ \equiv k_{T\cdot SM}$ or $k_{TM\cdot S}$, depending on the dominant pathway to T·S*·M formation. From a fit of this expression to the data in Fig. 3, we can roughly estimate the constants. The saturating speed of $\sim$20 μm/min implies $r_t \sim 100$ dimer subunits added per second, for given $d = 3$ nm. The half-maximum speed, where $r_t = k_+[S]_0$ at $\sim$50% fractional dilution, implying $[S]_0 \cong 2r_t/k_+$ at no dilution. If $k_+ \sim 10$ $\mu M^{-1}s^{-1}$, similar to the binding rate constant for actin assembly, then $[S]_0 \sim 10$ μM, a reasonable value for a cytoplasmic protein concentration in a cell extract.

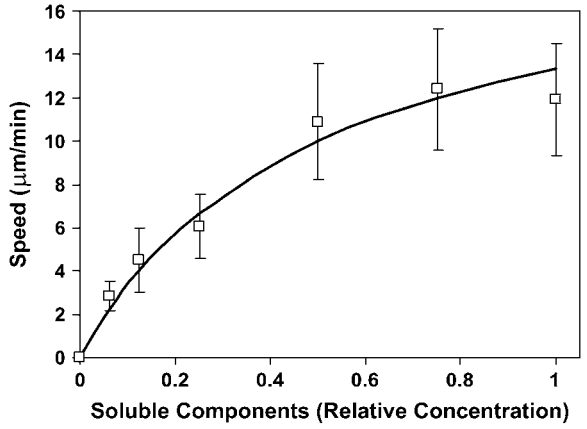

FIGURE 3 Plot of cell speed versus relative concentration of cytoplasmic proteins (reported by Italiano et al. 1996. Cell. 84:105–14, as fractional dilution of cell extract), showing a saturating dependence, which is characteristic of Michaelis-Menten kinetics. The solid line shows a fit of Eq. 11 to the data of Italiano et al.

Effects of force on MSP polymerization

When polymerization of either Mechanism-1 or -2 works against a force F (or operates under tension, in which case F is negative), the additional work required for the polymerization will affect the thermodynamics and potentially the kinetics of polymerization. The net free-energy change accounting for the work against the force F is

$$\Delta G(F) = \Delta G(F = 0) + Fd, \tag{15}$$

where d is the added length of the MSP filament per subunit ($\sim$3 nm). The thermodynamic stall force $F_{\max}$ is taken as the limiting force required to make the end-tracking cycle, up the point of tracking-unit release, energetically unfavorable is given by

$$F_{\max}d = kT\ln\frac{[\mathrm{M}]}{f[\mathrm{M}]_c} \leq -\Delta G_{\mathrm{ATP}\rightarrow\mathrm{ADP}} - kT\ln\frac{[\mathrm{M}]_c}{[\mathrm{M}]} - kT\ln\frac{[ATP]}{[ADP]K_h}, \tag{16}$$

with the right-hand side of the inequality arising from Eq. 6. The first term to the right of the inequality is $\sim$22 kT, and the energy involved in the second term to the right of the inequality need not be largely negative to facilitate rapid depolymerization and rapid reactivation of T. For example, having high driving forces of [ATP]/[ATP]K_h $\sim$ 100 and $[\mathrm{M}]_c/[\mathrm{M}]$ $\sim$ 100 would require only 9 kT of the $\sim$22 kT available from ATP hydrolysis, thus still allowing a high thermodynamic stall force of $\sim$18 pN.

Because $F_{\max}$ is so large, force will likely hinder the cycle kinetically well under this limit. Force may kinetically influence any of the reaction steps, thus making one or more of the various equilibrium parameters force dependent. However, unlike with a free-filament thermal ratchet mechanism (10,17), which predicts a subunit binding-rate constant of the form $k_{\mathrm{on}} = k_{\mathrm{on}}(F = 0)e^{-Fd/kT}$, force is not expected to affect binding of M or S* from solution to the end-tracking protein, or the rate of T·M activation in Mechanism-1. Rather, the force is expected to affect one or more of the subsequent steps in the net end-tracking cycle.

To estimate how the net rate r might depend on force, F, we show in the Appendix that the force-dependent transfer rate $r_t(F)$ has the approximate form

$$r_t(F) = r_t(F = 0)e^{-\alpha Fd/kT}, \tag{17}$$

where $\alpha = 1$ for highly flexible tracking units, and $\alpha = 1/2$ for very stiff tracking units. This implies the net rate (again assuming irreversible binding and transfer steps) has the approximate form

$$r \approx \frac{r_c}{1 + \dfrac{r_c}{r_t(F = 0)}e^{\alpha Fd/kT}}. \tag{18}$$

This predicted force-dependent polymerization rate is plotted in Fig. 4 for various values of $r_t(F = 0)/r_c$, revealing the characteristic kinetic behavior predicted by the end-tracking motor model. For filaments under lower forces or tension, the rate of polymerization is predicted to be independent of F when the transfer rate r_t is intrinsically much faster than the rate of dimer binding to the tracking unit. Only when forces are sufficiently large to slow this step in the cycle would polymerization be slowed. Conversely, when $r_t(F = 0)/r_c$ is small, the rate is predicted to be sensitive to force at smaller loads.

This idealized force-sensitivity analysis considers only the polymerization rate for a given local dimer concentration and

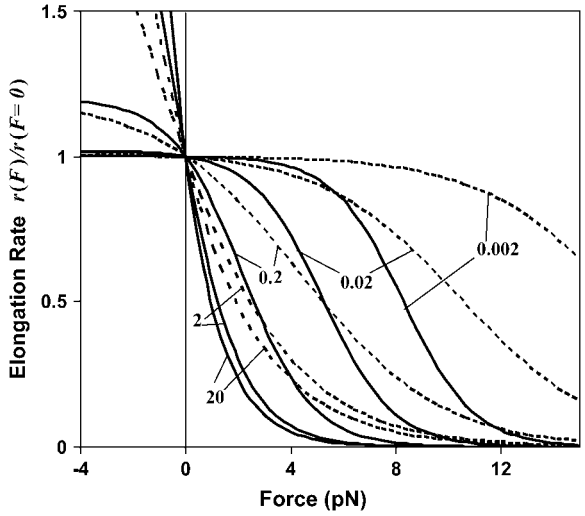

FIGURE 4 The predicted polymerization rate versus force, F, for various indicated values of the ratio r_c/r_t of the dimer-binding rate r_c to the dimer-transfer rate, r_t, calculated from Eq. 19. Results are shown for $\alpha = 1$ (*solid line*) reflecting flexible end-tracking proteins, and $\alpha = 1/2$ (*dashed line*) reflecting stiff end-tracking proteins.

ignores other potentially relevant limiting effects on force generation and the velocity of the membrane, such as changes in filament orientation (e.g., buckling) or diffusion limitations. The ability of filaments to transmit the polymerization energy to produce work on the membrane will depend on filament-filament interactions and the filament stiffness. Filament bundling should facilitate transmission of polymerization forces to the membrane, and bundling could possibly separately contribute the net force (18). Also, as the different values of α for stiff versus flexible tracking units demonstrate, it may be possible that tracking proteins are structurally optimized for force-insensitivity, such that $\alpha \sim 0$ for the dimer-transfer step, and the effect of force is felt by other (faster) steps in the cycle. In such a case, the force-insensitive plateau may extend over a greater range of compressive forces (4).

DISCUSSION

Two basic end-tracking mechanisms have been treated in detail here: Mechanism-1 with the membrane-bound tracking unit possessing ATPase activity, and Mechanism-2, where the ATPase activity is associated with a soluble cofactor. These cycles are analogs to end-tracking mechanisms for actin-based motility described previously by Dickinson et al. (4). In agreement with experimental observations of Italiano et al. (12) (Fig. 3), both mechanisms predict saturating Michaelis-Menten kinetics for polymerization rate as a function of soluble extract protein concentration. For Mechanism-1, filament elongation is rate limited at low extract concentrations by the concentration of a soluble enzyme E that uses ATP to activate the tracking unit-dimer (T·M) complex. For Mechanism-2, elongation is rate limited by the concentration of a soluble cofactor S that is activated by ATP and participates in the end-tracking cycle.

Although these two cycles are presented to illustrate how processive dimer addition and force generation might be achieved on MSP filaments tethered to the membrane, related end-tracking mechanisms cannot be excluded. For example, MSP dimers may bind directly to the filament, thereby triggering ATP hydrolysis and tracking-unit release (see Mechanism-A in Dickinson et al. (4)). Other variations with the energy released upon deactivation going instead to facilitate assembly at other steps of the end-tracking cycles are also plausible. For example, deactivation might instead go to increase affinity of T·M for F (i.e., decrease $K_{(TM)\cdot F}$ relative to $K_{(TM)^*\cdot F}$), in which case T could then be activated independently (T to T*) without necessarily promoting the reverse step of T* binding to F.

End-tracking motors may explain several properties of MSP-based motility. First, filament end-tracking motors explain why ATP is required and how it might be exploited. By directly capturing ATP hydrolysis energy for the net cycle of subunit addition to filament ends located at the membrane, assembly is thermodynamically favored exclusively for those filaments located at the membrane, as suggested by experimental observations (12). Second, processive MSP dimer addition by filament end-tracking motors explains the persistent tethering and attachment of filaments to propelled vesicles during filament assembly (12). Third, this model identifies potential roles for additional membrane-bound and soluble components (known to be required and to be rate limiting for MSP-based motility (12)) as ATPases that drive affinity-modulated interactions. Finally, these subunit-addition cycles by end-tracking proteins would explain the observed rate saturation of the motility rate with respect to solution-phase MSP dimer concentration, namely that the soluble or surface-bound ATPase components are saturated at high solution-phase MSP dimer concentrations.

In addition to providing explanations for above observations, the end-tracking motor concept is attractive in that it offers essentially the same underlying molecular mechanism for both MSP- and actin-based force generation, in light of the clear qualitative similarities between nematode sperm cell crawling and actin-based cell locomotion, and between MSP propulsion of vesicles and actin-based particle propulsion. Once the thermodynamic driving force and mechanism of synthesis of end-tethered filaments from the membrane to generate a moving MSP gel front are explained, the underlying mechanism for protrusive force generation is provided, as long as the generated MSP filament network is sufficiently rigid to bear the load. However, a full predictive model for cell crawling, involving MSP gel expansion and contraction, also requires a treatment of MSP filament network mechanics/dynamics. In this sense, the MSP end-tracking hypothesis proposed here potentially complements published sol-gel theories for nematode sperm cell crawling (11,18), despite our much-different assumptions about the mechanism of filament assembly at the cell membrane (i.e., processive assembly versus assembly of free ends and a Brownian ratchet-like bundling mechanism of MSP filaments into fibers). For example, the mechanism of MSP gel contraction is addressed by the sol/gel models, but only expansive forces are considered here, although end-tracking proteins might explain how MSP filaments remain attached to the membrane during both protrusion and contraction. Nevertheless, in the end-tracking model, polymerization of persistently tethered filaments should be the primary driving force for network expansion (i.e., protrusive forces), whereas filament-filament interactions such as cross-linking and bundling, which certainly affect the transduction of filament polymerization forces into membrane pressure, are of secondary importance.

Filament assembly and force generation by filament end-tracking motors would provide an inherently more efficient pathway than the previous proposal that MSP dimers become activated by a membrane component to form short-lived polymerization-competent intermediates that must diffusively find and bind filament ends before deactivating spontaneously (9). Filament end trackers ensure all activated subunits are incorporated at growth sites on the membrane. As first argued from theory (3) and subsequently demonstrated

experimentally (19,20), filaments need not be free-ended to allow subunit addition and force generation, contrary to what was widely assumed on the basis of the free-filament thermal (Brownian) ratchet models (10,17,21). Indeed, end-tracking motors should have clear mechanical and kinetic advantages for force generation compared to pushing by free-ended filament in a thermal ratchet mechanism (4). The persistent linkage of membrane-bound end trackers to filaments could transmit both protrusive and retractive forces during cell crawling. Importantly, there is mounting structural (22) and biochemical (14,19,20) evidence that the filament end-tracking mechanism adequately describes how actin filaments can elongate and generate force while persistently tethered at their elongating ends. MSP filaments may similarly elongate and push while tethered to the motile surface, contrary to what is assumed in some previous models for nematode sperms cell motility (11,18).

Whether the actual MSP-addition cycle in motile nematode sperm cells resembles one of the filament-end tracking mechanisms described here remains to be determined. At a minimum, our alternative mechanistic description of how MSP could be driven by an essentially analogous enzymatic cycle as that proposed for actin-based motility (except for the location of the ATPase activity). This proposal may resolve the paradox of why MSP-based and actin-based motility appear to behave so similarly, despite obvious differences in subunit/polymer polarity and their ATP-binding properties. Because the principle of filament end-tracking motors (3,4) has been recently experimentally confirmed in the case of formins (14,19,20,23) this variation of the end-tracking mechanism merits close scrutiny for comprehending nematode sperm cell motility.

APPENDIX

Approximate kinetic expressions for end-tracking MSP polymerization

Here we examine the steady-state probability flux through the end-tracking cycle under the assumption that binding of the dimer M, soluble cofactor S, or complex S·M to the tracking unit and/or the MSP-dimer transfer steps are rate limiting. For simplicity, we assume the remaining transitions in the cycle occur quickly and are at equilibrium, and that reactivation of the tracking unit (or cofactor S) is strongly favored thermodynamically. Under these assumptions, the probability of finding the cycle in a state other than having only one tracking unit bound becomes negligible.

For Mechanism-1, we assume dimers are at a high enough concentration such that they bind rapidly to the tracking unit to form T·M at a rate that is fast compared to the rates of activation (i.e., (T·M)* formation) and dimer transfer (i.e., (T·M)*·F formation). We further assume the activation rate is proportional to the concentration of a soluble activation enzyme, E. Let p be the probability of finding the tracking unit as (T·M)*. The balance equation for p is

$$\frac{dp}{dt} = k_a[\mathrm{E}](1-p) - k_{(\mathrm{TM})*\cdot\mathrm{F}}p, \tag{A-1}$$

which has the steady-state solution,

$$r = k_{(\mathrm{TM})*\cdot\mathrm{F}}p = \frac{k_a[\mathrm{E}]}{1+\dfrac{k_a[\mathrm{E}]}{k_{(\mathrm{TM})*\cdot\mathrm{F}}}}. \tag{A-2}$$

The rate r is therefore a saturating function of [E], displaying Michaelis-Menten kinetics with r asymptotically approaching $k_{(\mathrm{TM})*\cdot\mathrm{F}}$ for $[\mathrm{E}] \gg k_{(\mathrm{TM})*\cdot\mathrm{F}}/k_a$. Equation A-2 can be written

$$r = \frac{r_b}{1+\dfrac{r_b}{r_t}}, \tag{A-3}$$

where $r_b \equiv k_a[\mathrm{E}]$ is the activation rate and $r_t \equiv k_{(\mathrm{TM})*\cdot\mathrm{F}}$ is the dimer transfer rate. The net elongation rate is limited by the slowest of these two rates; i.e., when $r_b \ll r_t$, then $r \approx r_b$, and when $r_b \gg r_t$, then $r \approx r_t$.

We can draw similar conclusions about Mechanism-2, although the analysis is complicated by the various potential pathways to forming the T·S*·M complex. We will specifically consider the following limiting cases: a), S* binds M in solution to saturation of S* ($[\mathrm{M}] \gg K_{\mathrm{S}*\cdot\mathrm{M}}$), and only the S*·M complex binds to T ($[\mathrm{S}*] \ll K_{\mathrm{T}\cdot\mathrm{S}*}$; $[\mathrm{M}] \ll K_{\mathrm{T}\cdot\mathrm{M}}$); and b), S* cannot bind M in solution ($[\mathrm{M}] \ll K_{\mathrm{S}*\cdot\mathrm{M}}$), and M cannot bind T without S being first bound to T ($[\mathrm{M}] \ll K_{\mathrm{T}\cdot\mathrm{M}}$). We assume that the solution-phase reactions are rapid and again assume ATP activation of S and tracking-unit dissociation from the filament following deactivation are rapid and irreversible.

For case a), let p be the probability of the cycle being in the state with T·S*·M complex having formed. The balance equation on p is

$$\frac{dp}{dt} = k_{\mathrm{T}\cdot\mathrm{S}^*\mathrm{M}}[\mathrm{S}^*\cdot\mathrm{M}](1-p) - k^-_{\mathrm{T}\cdot\mathrm{S}^*\mathrm{M}}p - k_{\mathrm{TS}^*\mathrm{M}\cdot\mathrm{F}}p, \tag{A-4}$$

which has the same form as Eq. A-1; therefore

$$r = k_{\mathrm{TS}^*\mathrm{M}\cdot\mathrm{F}}p = \frac{k_{\mathrm{T}\cdot\mathrm{S}^*\mathrm{M}}[\mathrm{S}^*\cdot\mathrm{M}]}{1+\dfrac{k_{\mathrm{T}\cdot\mathrm{S}^*\mathrm{M}}([\mathrm{S}^*\cdot\mathrm{M}]+K_{\mathrm{T}\cdot\mathrm{S}^*\mathrm{M}})}{k_{\mathrm{TS}^*\mathrm{M}\cdot\mathrm{F}}}}. \tag{A-5}$$

For $[\mathrm{S}*\cdot\mathrm{M}] \gg K_{\mathrm{S}\cdot\mathrm{M}}$, all steps are approximately irreversible, and

$$r \cong \frac{k_{\mathrm{T}\cdot\mathrm{S}^*\mathrm{M}}[\mathrm{S}^*\cdot\mathrm{M}]}{1+\dfrac{k_{\mathrm{T}\cdot\mathrm{S}^*\mathrm{M}}[\mathrm{S}^*\cdot\mathrm{M}]}{k_{\mathrm{TS}^*\mathrm{M}\cdot\mathrm{F}}}}, \tag{A-6}$$

which again has the form of Eq. A-3, but with $r_b \equiv k_{\mathrm{T}\cdot\mathrm{S}^*\mathrm{M}}[\mathrm{S}^*\cdot\mathrm{M}]$ and $r_t \equiv k_{\mathrm{TS}^*\mathrm{M}\cdot\mathrm{F}}$. For large dimer concentration, $[\mathrm{M}] \gg K_{\mathrm{S}*\cdot\mathrm{M}}$, and strong driving force for activation, such that $[\mathrm{S}*] \gg [\mathrm{S}]$, then nearly all S is in the bound activated form, such that $[\mathrm{S}*\cdot\mathrm{M}] \cong [\mathrm{S}]_0$, where $[\mathrm{S}]_0$ is the total solution-phase concentration of S. In this limit, $r_b \equiv k_{\mathrm{T}\cdot\mathrm{SM}}[\mathrm{S}]_0$.

For limiting case b), let p_1 be the probability of having only S* bound to the tracking unit, and p_2 be the probability of both S* and M bound.

$$\begin{aligned}\frac{dp_1}{dt} &= k_{\mathrm{T}\cdot\mathrm{S}^*}[\mathrm{S}^*](1-p_1-p_2) - k^-_{\mathrm{T}\cdot\mathrm{S}^*}p_1 - k_{\mathrm{TS}^*\cdot\mathrm{M}}[\mathrm{M}]p_1 + k^-_{\mathrm{TS}^*\cdot\mathrm{M}}p_2\\ \frac{dp_2}{dt} &= k_{\mathrm{TS}^*\cdot\mathrm{M}}[\mathrm{M}]p_1 - k^-_{\mathrm{TS}^*\cdot\mathrm{M}}p_2 - k_{\mathrm{TS}^*\mathrm{M}\cdot\mathrm{F}}p_2.\end{aligned} \tag{A-7}$$

Solving for p_2 at steady-state yields

$$r = k_{\mathrm{TS}^*\mathrm{M}\cdot\mathrm{F}}p_2 = \frac{k_{\mathrm{TS}^*\mathrm{M}\cdot\mathrm{F}}k_{\mathrm{T}\cdot\mathrm{S}^*}[\mathrm{S}^*]k_{\mathrm{TS}^*\cdot\mathrm{M}}[\mathrm{M}]}{(k_{\mathrm{T}\cdot\mathrm{S}^*}[\mathrm{S}^*]+k^-_{\mathrm{T}\cdot\mathrm{S}^*})(k^-_{\mathrm{TS}^*\cdot\mathrm{M}}+k_{\mathrm{TS}^*\mathrm{M}\cdot\mathrm{F}})+k_{\mathrm{TS}^*\cdot\mathrm{M}}[\mathrm{M}](k_{\mathrm{T}\cdot\mathrm{S}^*}[\mathrm{S}^*]+k_{\mathrm{TS}^*\mathrm{M}\cdot\mathrm{F}})}. \tag{A-8}$$

In the limit of large [M], this becomes

$$r = \frac{k_{T\cdot S^*}[S^*]}{1 + \frac{k_{T\cdot S^*}[S^*]}{k_{TS^*M\cdot F}}}, \tag{A-9}$$

which again has the form of Eq. A-3, with $r_b \equiv k_{T\cdot S}[S^*]$ and $r_t \equiv k_{TMS\cdot F}$. For $[S^*] \gg [S]$, then $[S^*] \cong [S]_0$ and $r_b \equiv k_{T\cdot S}[S]_0$.

Limiting expressions for force-dependent MSP dimer-transfer rate

Here we justify our expectation that the MSP dimer transfer rate, r_t, in the end-tracking Mechanisms-1 and -2 (Fig. 2) should have approximately the form

$$r_t(F) = r_t(F = 0)e^{-\alpha Fd/kT}, \tag{A-10}$$

where $\alpha = 1$ for highly flexible tracking units, and $\alpha = 1/2$ for stiff spring-like tracking units.

For highly flexible tracking units, the binding domain of the tracking unit can move freely within a molecular length b from the membrane surface, as reflected by a square-well potential, $\phi(z) = 0$ for $0 \le z \le b$, $\phi(z) = \infty$ for $z < 0$ and $z > b$. A bound tracking unit under force F will therefore assume the stationary Boltzmann density,

$$p(z) = \frac{F}{kT}\frac{e^{-Fz/kT}}{1 - e^{-Fb/kT}}. \tag{A-11}$$

Because binding sites of the adjacent filaments are offset by the distance d, the other free tracking unit can transfer a new MSP dimer to the filament end only if $z > d$ for the filament-bound tracking unit; otherwise, the potential energy of the newly bound tracking unit would be ∞ upon binding. In other words, fluctuations in z must free up a gap of width d to allow addition of the next MSP dimer. Therefore, r_t is proportional to the stationary probability of finding $z > d$, which is

$$\mathrm{Prob}(z > d) = \int_d^b p(z)dz = \frac{e^{-Fd/kT} - e^{-Fb/kT}}{1 - e^{-Fb/kT}}. \tag{A-12}$$

For larger forces F or molecular lengths b, such that $Fb \gg kT$, this becomes

$$\mathrm{Prob}(z > d) \approx e^{-Fd/kT}, \tag{A-13}$$

resulting in Eq. A-10 with $\alpha = 1$.

For a stiff spring-like molecule, with $\phi(z) = \frac{\kappa}{2}(z - z_0)^2$ where κ is the molecular stiffness, then the force-dependent probability density of the bound tracking unit is,

$$p(z) = \frac{1}{\sqrt{2\pi kT/\kappa}}e^{-\frac{\kappa}{2kT}(z - z_{eq})^2}, \tag{A-14}$$

where $z_{eq} = z_0 - F/\kappa$. This expression assumes the tracking units are sufficiently stiff, such that the membrane barrier is effectively at infinite distance relative to possible deflection distances of the tracking-unit binding position. Equation A-15 (below) describes the joint probability of finding the second tracking unit at the position $z_2 = z - d$ when the first bound unit is at any position $z_1 = z$.

$$p(z_2 = z - d, z_1 = z) = \frac{1}{2\pi kT/\kappa}e^{-\frac{\kappa}{2kT}(z - z_{eq})^2}e^{-\frac{\kappa}{2kT}(z - d - z_0)^2}. \tag{A-15}$$

The MSP dimer transfer rate is proportional to this quantity, integrated over all positions z, resulting in

$$\mathrm{Prob}(z_2 = z_1 - d) = \int_{-\infty}^{\infty} p(z_2 = z - d, z_1 = z)dz = \frac{1}{2\sqrt{\pi kT/\kappa}}e^{-(\kappa d^2/4 + Fd/2 + F^2/4\kappa)/kT}, \tag{A-16}$$

hence, $r_t(F) = r_t(F = 0)e^{-F(d + F/2\kappa)/2kT}$. In the limit of high stiffness or low force, where the force-induced deflection of the bound tracking unit is small compared to the lattice spacing on the filament, i.e., $F/2\kappa \ll d$, then Eq. A-1 is obtained, with $\alpha = 1/2$.

This work was supported with funding from grants from the National Science Foundation (CTS-0505929), and the National Institutes of Health (R01-GM067828).

REFERENCES

1. Bray, D. 2001. Cell Movements: From Molecules to Motility. Garland Publishing, New York.
2. Wegner, A., and J. Engel. 1975. Kinetics of the cooperative association of actin to actin filaments. *Biophys. Chem.* 3:215–225.
3. Dickinson, R. B., and D. L. Purich. 2002. Clamped-filament elongation model for actin-based motors. *Biophys. J.* 82:605–617.
4. Dickinson, R. B., L. Caro, and D. L. Purich. 2004. Force generation by cytoskeletal filament end-tracking proteins. *Biophys. J.* 87:2838–2854.
5. Stewart, M., T. M. Roberts, J. E. Italiano Jr., K. L. King, R. Hammel, G. Parathasathy, T. L. Bullock, A. J. McCoy, H. Kent, A. Haaf, and D. Neuhaus. 1998. Amoeboid motility without actin: insights into the molecular mechanism of locomotion using the major sperm protein (MSP) of nematodes. *Biol. Bull.* 194:342–343 (discussion 343–344).
6. Roberts, T. M., and M. Stewart. 2000. Acting like actin. The dynamics of the nematode major sperm protein (msp) cytoskeleton indicate a push-pull mechanism for amoeboid cell motility. *J. Cell Biol.* 149: 7–12.
7. Bullock, T. L., A. J. McCoy, H. M. Kent, T. M. Roberts, and M. Stewart. 1998. Structural basis for amoeboid motility in nematode sperm. *Nat. Struct. Biol.* 5:184–189.
8. Italiano, J. E. Jr., M. Stewart, and T. M. Roberts. 2001. How the assembly dynamics of the nematode major sperm protein generate amoeboid cell motility. *Int. Rev. Cytol.* 202:1–34.
9. Roberts, T. M., E. D. Salmon, and M. Stewart. 1998. Hydrostatic pressure shows that lamellipodial motility in Ascaris sperm requires membrane-associated major sperm protein filament nucleation and elongation. *J. Cell Biol.* 140:367–375.
10. Mogilner, A., and G. Oster. 1996. Cell motility driven by actin polymerization. *Biophys. J.* 71:3030–3045.
11. Bottino, D., A. Mogilner, T. Roberts, M. Stewart, and G. Oster. 2002. How nematode sperm crawl. *J. Cell Sci.* 115:367–384.
12. Italiano, J. E. Jr., T. M. Roberts, M. Stewart, and C. A. Fontana. 1996. Reconstitution in vitro of the motile apparatus from the amoeboid sperm of Ascaris shows that filament assembly and bundling move membranes. *Cell.* 84:105–114.
13. LeClaire 3rd, L. L., M. Stewart, and T. M. Roberts. 2003. A 48 kDa integral membrane phosphoprotein orchestrates the cytoskeletal dynamics that generate amoeboid cell motility in Ascaris sperm. *J. Cell Sci.* 116:2655–2663.

14. Romero, S., C. Le Clainche, D. Didry, C. Egile, D. Pantaloni, and M. F. Carlier. 2004. Formin is a processive motor that requires profilin to accelerate actin assembly and associated ATP hydrolysis. *Cell*. 119: 419–429.

15. Miao, L., O. Vanderlinde, M. Stewart, and T. M. Roberts. 2003. Retraction in amoeboid cell motility powered by cytoskeletal dynamics. *Science*. 302:1405–1407.

16. Buttery, S. M., G. C. Ekman, M. Seavy, M. Stewart, and T. M. Roberts. 2003. Dissection of the Ascaris sperm motility machinery identifies key proteins involved in major sperm protein-based amoeboid locomotion. *Mol. Biol. Cell*. 14:5082–5088.

17. Peskin, C. S., G. M. Odell, and G. F. Oster. 1993. Cellular motions and thermal fluctuations: the Brownian ratchet. *Biophys. J*. 65:316–324.

18. Wolgemuth, C. W., L. Miao, O. Vanderlinde, T. Roberts, and G. Oster. 2005. MSP dynamics drives nematode sperm locomotion. *Biophys. J*. 88:2462–2471.

19. Higashida, C., T. Miyoshi, A. Fujita, F. Oceguera-Yanez, J. Monypenny, Y. Andou, S. Narumiya, and N. Watanabe. 2004. Actin polymerization-driven molecular movement of mDia1 in living cells. *Science*. 303:2007–2010.

20. Kovar, D. R., and T. D. Pollard. 2004. Insertional assembly of actin filament barbed ends in association with formins produces piconewton forces. *Proc. Natl. Acad. Sci. USA*. 101:14725–14730.

21. Hill, T. L. 1981. Microfilament or microtubule assembly or disassembly against a force. *Proc. Natl. Acad. Sci. USA*. 78:5613–5617.

22. Chereau, D., and R. Dominguez. 2006. Understanding the role of the G-actin-binding domain of Ena/VASP in actin assembly. *J. Struct. Biol*. 155:195–201.

23. Zigmond, S. H., M. Evangelista, C. Boone, C. Yang, A. C. Dar, F. Sicheri, J. Forkey, and M. Pring. 2003. Formin leaky cap allows elongation in the presence of tight capping proteins. *Curr. Biol*. 13:1820–1823.

24. Italiano J. E., M. Stewart, and T. M. Roberts. 1999. Localized depolymerization of the major sperm protein cytoskeleton correlates with the forward movement of the cell body in the amoeboid movement of nematode sperm. *J. Cell Biol*. 146:1087–1095.